JOURNAL OF SPACECRAFT AND ROCKETS
Vol. 34, No. 2, March–April 1997

Mission Performance and Design Sensitivities of Air-Breathing Hypersonic Launch Vehicles

David K. Schmidt* and T. Alan Lovell†
University of Maryland, College Park, Maryland 20742

Hypersonic vehicles with single-stage-to-orbit capability present a major system design challenge. Maximum system efficiency is required to achieve the mission objective, and this clearly depends in some way on subsystem efficiencies, including structural, aerodynamic, propulsive, and operational. Because all subsystem efficiencies are interrelated, especially for these vehicles, a design based on independent optimization of the subsystems will not lead to the optimum system. A system analysis will be performed in the attempt to determine sensitivities between subsystem efficiencies and mission performance. Trajectory optimization is the basic tool used to determine maximum orbital mass fraction for a specified orbit-injection mission. Then parametric analysis of basic efficiencies and sizing parameters are performed, a matrix of configurations generated, and their mission performance determined. The key results from this analysis include the formulation of the problem for this vehicle class using trajectory optimization, the characteristics of the optimal trajectories, and the subsystem sensitivities. Results indicate that the maximum achievable orbital mass fraction is a stronger function of propulsion-system efficiencies than the vehicle's aerodynamic efficiency. Thus, a mission-performance-optimized configuration would tend to have low slenderness ratio, with propulsive capability stressed over aerodynamic efficiency.

Nomenclature

A_d	= engine diffuser area ratio
A_e	= engine exit area, ft^2
A_n	= engine nozzle area ratio
C_D	= vehicle drag coefficient
C_{D_0}	= parasite drag coefficient
C_L	= aerodynamic lift coefficient
c_p	= specific heat at constant pressure, Btu/lb-°R
D	= aerodynamic drag, lb
E	= energy height, ft
g	= gravitational constant, ft/s^2
H_E	= engine nozzle exit height, ft
H_i	= engine inlet height, ft
h	= altitude above Earth's surface, ft
I_{sp}	= specific impulse, s
L	= aerodynamic lift, lb
l_1	= vehicle forebody length, ft
l_2	= vehicle afterbody length, ft
l_3	= vehicle total length, ft
M	= Mach number
M_1, p_1, T_1	= engine inlet conditions
M_2, p_2, T_2	= combustor inlet conditions
M_3, p_3, T_3	= combustor exit conditions
$M_4(=M_e)$, $p_4(=p_e)$, $T_4(=T_e)$	= engine exit conditions
$\dot{m}_f$	= fuel mass flow rate, slugs/s
p	= atmospheric or working fluid static pressure, psf
p_{fb}	= surface pressure on vehicle forebody, psf
p_t	= total pressure, psf
p_{us}	= pressure on upper surface of vehicle, psf
$\dot{Q}$	= stagnation heat transfer rate, Btu/ft^2/s
Q_r	= heating value of the fuel, Btu/lb
q	= dynamic pressure, psf
R	= universal gas constant, 1716 ft^2/s^2/°R
R_e	= radius of Earth, ft
T	= atmospheric or working fluid static temperature, °R
Th	= thrust, lb
V	= velocity, ft/s
W	= total vehicle weight, lb
W_a	= effective forebody width, ft
W_{ab}	= effective afterbody width, ft
$\dot{W}_f$	= fuel flow rate (by weight), lb/s
W_p	= effective propulsive width, ft
X_{plume}, Z_{plume}	= force due to exhaust plume pressure distribution, lb
Z_{turn}	= force due to turning of flow at engine inlet, lb
α	= vehicle angle of attack, deg
γ	= vehicle flight-path angle, deg; ratio of specific heats
η_a	= aerodynamic efficiency
η_c	= combustion efficiency
η_d	= diffuser efficiency
η_e	= afterbody/nozzle expansion efficiency
η_m	= mass capture efficiency
η_n	= nozzle efficiency
ρ	= atmospheric or working fluid density, slugs/ft^3
τ_1	= forebody nose angle, deg
τ_2	= afterbody nose angle, deg

Subscripts

i	= inlet
t	= total
∞	= freestream condition

Received Oct. 4, 1995; revision received Oct. 1, 1996; accepted for publication Oct. 1, 1996.

*Professor of Aerospace Engineering and Director, Flight Dynamics and Control Laboratory. Associate Fellow AIAA.

†Graduate Research Assistant, Flight Dynamics and Control Laboratory, and Graduate Student, Department of Aerospace Engineering. Student Member AIAA.

Introduction

A POSSIBLE next-generation launch vehicle will be a fully reusable, single-stage-to-orbit (SSTO) aerospacecraft. A typical generic configuration may use liquid hydrogen (LH_2) fuel, be 150 ft in length, have a gross weight between 300,000 and 500,000 lb, be capable of horizontal takeoff and landing, accelerate to Mach 25 in the upper atmosphere, and deliver payload into low earth orbit.[1]

To meet these mission requirements, the vehicle must utilize an air-breathing propulsion system for much of its trajectory to avoid the weight penalty of carrying the oxidizer. The air-breathing

scramjet engine may be the primary propulsive system, and to obtain maximum propulsive efficiency, the scramjet engine must be operated at a high-dynamic pressure. However, since aerodynamic heating and drag also increase with dynamic pressure, the benefits of high-propulsive efficiency must be balanced against temperature and structural constraints. Further, aerodynamic and propulsive performance (e.g., L/D, thrust, and fuel flow) vary with vehicle weight, Mach number, and altitude, and so the vehicle performance (i.e., maximum payload to orbit) will depend on the vehicle trajectory. Similarly, both aerodynamic forces and heating are functions of Mach number and altitude; thus, aerodynamic efficiency and structural design requirements (e.g., the amount of aerodynamic heating the structure can withstand) are trajectory dependent as well. Consequently, independent subsystem optimization will not lead to the optimal integrated system.[2,3]

Because these vehicles are neither conventional aircraft nor rockets the vehicle sizing problem is unique. Conventional aircraft sizing, based on Breguet analysis, for example, is not appropriate, nor is classic rocket performance analysis. Consequently, the sizing problem must be reformulated.

First, the formulation of the sizing problem, using trajectory optimization, will be presented, along with a brief description of the baseline vehicle configuration. Next, motivation is provided for determining the key performance drivers, followed by an in-depth discussion of several vehicular subsystems, which are potentially the most critical. Finally, a parametric analysis will be performed to determine the relationship between mission performance and subsystem efficiencies.

Generic Vehicle Description

The vehicle geometry considered was selected to reflect key characteristics similar to those of the X-30 vehicle.[1] The configuration is a lifting body, with an air-breathing, hydrogen-fueled propulsion system (scramjet). The basic geometry is shown in Fig. 1. The configuration consists of a forebody/engine inlet, internal engine module, and afterbody/exhaust nozzle. The weight of the vehicle at scramjet ignition will be taken to be 300,000 lb.

The vehicle's forebody provides not only aerodynamic lift but also precompression for the engine module. As a result, the properties of the air flowing into the combustor, and thus the overall engine performance, are strong functions of both the forebody geometry and vehicle attitude (i.e., angle of attack). Further, the afterbody acts as a nozzle extension that experiences exhaust-plume impingement. The resulting pressure distribution on the afterbody generates propulsive thrust and lift, as well as pitching moment. An additional aeropropulsive effect is the download on the engine inlet cowl as the air incident on the forebody is redirected into the inlet.

The hydrogen-fueled scramjet engine includes three main sections, a variable-geometry diffuser, combustor, and internal expansion nozzle, as shown in Fig. 2. Station 1 denotes the engine inlet, station 2 the diffuser exit/combustor inlet, station 3 the combustor exit/nozzle inlet, and station 4 the engine exit.

The relevant aerodynamic forces are the lift and drag on the forebody and upper surface. These forces can be expressed,[4] for example, as

$$L = l_1 W_a p_{\mathrm{fb}}(\alpha)\cos(\alpha+\tau_1) - l_3 W_a p_{\mathrm{us}}(\alpha)\cos\alpha$$
$$D = l_1 W_a p_{\mathrm{fb}}(\alpha)\sin(\alpha+\tau_1) - l_3 W_a p_{\mathrm{us}}(\alpha)\sin\alpha + l_1 W_a q_\infty C_{D_0} \tag{1}$$

and the coefficients

$$C_L = L/(q_\infty S) \qquad C_D = D/(q_\infty S)$$

may be defined in terms of the aerodynamic reference area

$$S = l_1 W_a$$

Figure 3 shows the resulting drag polar, assuming $C_{D_0} = 0.024$ independent of Mach number, and Fig. 4 shows the resulting lift-to-drag ratio. The nonparabolic drag polar is typical of vehicles with the low-effective aspect ratio of a lifting body, where by nonparabolic we mean $C_D = C_{D_0} + K(C_L)^p$ and where p is less than two. The maximum L/D of about two corresponds to an angle of attack near 1 deg.

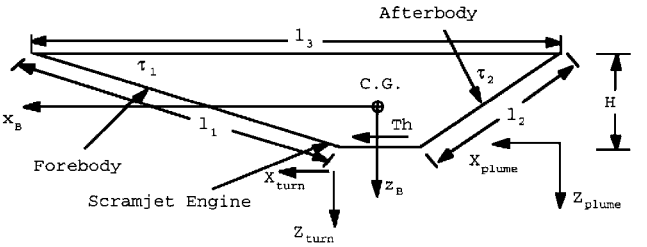

Fig. 1 Generic hypersonic lifting-body configuration.

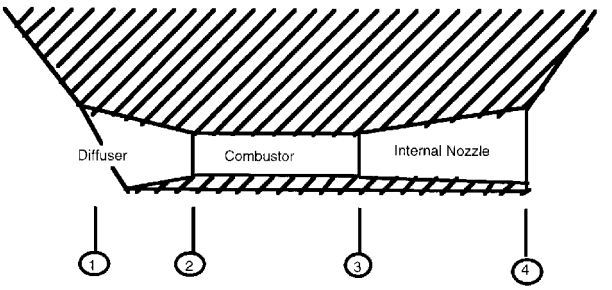

Fig. 2 Scramjet engine.

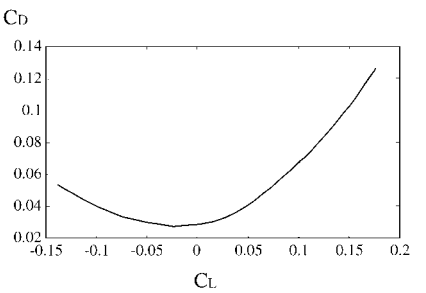

Fig. 3 Drag polar, baseline vehicle.

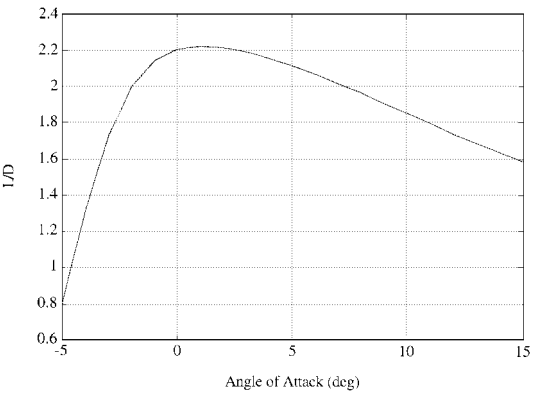

Fig. 4 Lift-to-drag ratio, baseline configuration.

Under Newtonian theory these data are not strong functions of Mach number, considering only the hypersonic Mach range ($M > 5$).

The engine inlet conditions depend not only on the flight Mach number and altitude but are also strongly dependent on the forebody angle of attack. Using Newtonian theory to estimate the inlet conditions, a cycle analysis for the engine was performed in Ref. 4, and an engine performance model developed. This propulsion-system model included two control limits. The first is a diffuser area ratio limit. For complete combustion to occur, a combustor inlet pressure of approximately 1 atm is suggested.[5] A variable geometry diffuser is assumed to deliver a constant combustor inlet pressure of 1 atm, subject to a maximum allowable diffuser area ratio of unity.[2,4,6] This feature was recommended in Refs. 2 and 6 to actively control the high-frequency pressure and Mach variation in the combustor for stable combustion. The second limit is on the fuel/air ratio (FAR). The maximum FAR is that which will thermally choke the combustor, subject to the maximum FAR corresponding to the stoichiometric value of 0.03 (Ref. 7). FARs above stoichiometric will not be considered here, though Ref. 8 suggests

that performance may be increased slightly if FARs above stoichiometric are considered. This will be examined further in later studies.

Subject to these limits, the cycle analysis yields the following relationships for fuel flow and propulsive thrust:

$$Th = \left\{ P_e\left[\gamma M_e^2 + 1\right] - \frac{P_1\left[\gamma M_1^2 \cos\tau_1 + 1\right]}{A_d A_n} \right\} A_e$$
$$\dot{m}_f = \frac{\dot{W}_f}{g} = P_1 M_1 \left(\sqrt{\frac{\gamma}{RT_1}}\right)\left(\frac{A_e}{A_d A_n}\right)(\text{FAR}) \tag{2}$$

which depend on $A_e = H_E W_p$. Here, Th is the thrust generated by the engine module not including plume expansion. The plume expansion leads to the forces

$$X_{\text{plume}} = P_\infty l_2 W_{\text{ab}}\left[\frac{\bar{P}\,\ell n(\bar{P})}{(\bar{P}-1)}\right]\sin\tau_2 \qquad \text{where} \qquad \bar{P} = \frac{P_e}{P_\infty}$$
$$Z_{\text{plume}} = -P_\infty l_2 W_{\text{ab}}\left[\frac{\bar{P}\,\ell n(\bar{P})}{(\bar{P}-1)}\right]\cos\tau_2 \tag{3}$$

which depend on W_{ab}. Finally, the forces on the engine inlet produced by redirecting the inlet airflow is given by

$$X_{\text{turn}} = \gamma P_1 M_1^2 [A_e/A_d A_n](1 - \cos\tau_1)$$
$$Z_{\text{turn}} = \gamma P_1 M_1^2 [A_e/A_d A_n]\sin\tau_1 \tag{4}$$

With reference to Fig. 1, total propulsive thrust and lift will then be defined, respectively, as

$$T_x = Th + X_{\text{plume}} + X_{\text{turn}} \qquad T_z = Z_{\text{plume}} + Z_{\text{turn}} \tag{5}$$

If coefficients C_{T_x} and C_{T_z} are defined as the propulsive forces nondimensionalized by flight dynamic pressure and the aerodynamic reference area, Fig. 5 shows these coefficients at 100,000-ft altitude. The values shown are typical, with coefficients corresponding to lower altitudes taking on smaller values. The main points with respect to these data are that these propulsive forces are strong functions of vehicle angle of attack and the propulsive lift is the same order of magnitude as, but in the opposite direction from, the aerodynamic lift.

Finally for this vehicle, and with reference to Fig. 1, the specific impulse may be defined to be

$$I_{\text{sp}} = \frac{1}{\dot{W}_f}\{(Th + X_{\text{plume}} + X_{\text{turn}})\cos\alpha + (Z_{\text{plume}} + Z_{\text{turn}})\sin\alpha\} \equiv \frac{Th_{\text{installed}}}{\dot{W}_f} \tag{6}$$

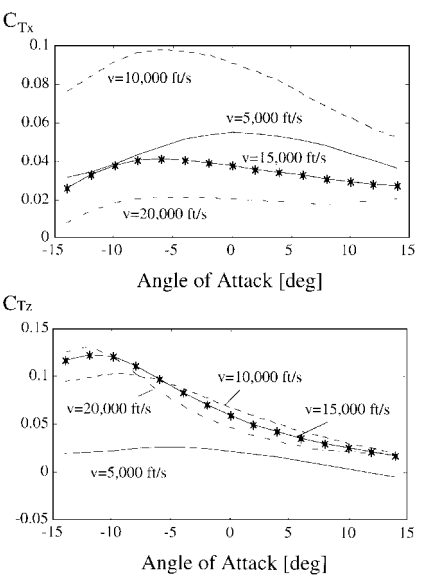

Fig. 5 Propulsive force coefficients, baseline configuration at h = 100,000 ft.

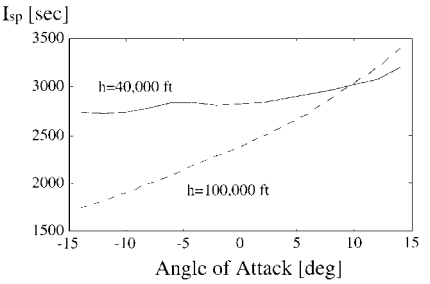

Fig. 6 Specific impulse for baseline configuration, V = 10,000 fps.

Note that this definition includes the component of thrust along the velocity vector, which is important for performance analysis. The strong dependence of propulsive performance on angle of attack is demonstrated in Fig. 6, which shows the specific impulse corresponding to a flight a velocity of 10,000 ft/s at two different altitudes. The angle-of-attack dependence is greater at higher altitudes, where the reduced atmospheric density magnifies the effect of the precompression from the forebody. Values for specific impulse at higher Mach numbers are typically greater than those shown in Fig. 6, due to higher inlet compression. Note that no inlet losses, perfect pressure recovery, and perfect fuel combustion are assumed in these data. Effects of reduced efficiencies will be estimated later.

Optimization Paradigm

As noted earlier, the feasibility of the SSTO mission clearly depends on the efficiencies of the vehicular subsystems, and system optimization will be required. In contrast to the investigations reported in Refs. 8–11, for example, the problem addressed here is not precise trajectory optimization for a given vehicle design. In this investigation we are interested in determining the key performance drivers for a class of systems prior to detailed design of a particular vehicle. Hence, we seek to determine a priori what is important in terms of mission performance, before a detailed vehicle description is available.

The prototypical mission is to deliver payload into circular low Earth orbit (LEO), with a typical orbital altitude of 200,000 ft. To gain fundamental insight, note first that this mission is one of gaining total energy E, where we define

$$E = [hR_e/(R_e + h)] + (V^2/2g_0) \tag{7}$$

(This expression is the sum of potential plus kinetic energies per unit weight. It is similar to the specific energy used in orbit mechanics, but the usage here is more typical in atmospheric flight mechanics.) A key relation is the rate at which the vehicle can increase energy, where

$$\dot{E} = \frac{(Th_{\text{installed}} - D)V}{W} \tag{8}$$

Under some assumptions,[12] the following approximation may be obtained (note that this approximation is made here to gain insight; the exact expression [Eq. (8)] is used in determining the numerical results presented later):

$$\mathrm{d}E \approx \frac{V}{\text{SFC}}\left[\frac{(T/WL/D - 1)}{(T/WL/D)}\right]\frac{\mathrm{d}W_f}{W} \tag{9}$$

which reveals a first-order approximation for the instantaneous mission-performance, the energy gained per unit of fuel $\mathrm{d}E/\mathrm{d}W_f$. The greater this efficiency, averaged over the mission, the greater the orbital mass fraction W_{final}/W_0 achievable, since the fuel required to achieve the desired orbital condition can be expressed as

$$W_f = \int_{E_0}^{E_f} \mathrm{d}W_f = \int_{E_0}^{E_f} \frac{\mathrm{d}E}{\mathrm{d}E/\mathrm{d}W_f} \tag{10}$$

and orbital mass fraction can be expressed as

$$\frac{W_{\text{final}}}{W_0} = \frac{W_{\text{payload}}}{W_0} + \frac{W_{\text{structure}}}{W_0} + \frac{W_{\text{inert system}}}{W_0} \tag{11}$$

So mission performance, measured in terms of maximum orbital mass fraction, is clearly a function of the aerodynamic efficiency (L/D), and propulsive efficiency [T/W and specific fuel consumption (SFC)]. Also, structural efficiency (as measured by structural mass fraction $W_{\text{structure}}/W_0$), along with weight of unused fuel, avionics, etc. (lumped in $W_{\text{inert system}}$), trades against payload mass fraction for a given orbital mass fraction. If the weight of a given configuration consisted of only fuel (i.e., no payload or structure), SSTO would certainly be achievable because $\dot{E}$ would tend to infinity. But such a system would place no payload into orbit. Thus, the performance objective is not to just achieve SSTO but to place the maximum payload into LEO. And since the aerodynamic and propulsive efficiencies are trajectory dependent, trajectory optimization is required.

The first problem then is to determine the maximum mission performance (orbital mass fraction) for a given baseline vehicle configuration. This problem is solved by finding the minimum-fuel trajectory, which leads to the maximum orbital mass fraction.

The second problem is to determine the mission-performance sensitivity to changes in subsystem efficiencies. To solve this problem, subsystem efficiencies will be defined and parametrically adjusted relative to the baseline, generating a matrix of configurations. Then the maximum orbital mass fractions will be determined for each of these configurations. The results from this parametric analysis will then include both the optimal trajectories for the family of vehicles in the matrix, along with the sensitivities of mission performance to variations in the subsystem efficiencies.

Energy-state methodology will be employed to determine the minimum-fuel trajectories. This methodology affords a simple graphical solution to the optimization problem and has been classically used in aircraft performance analysis (cf. Ref. 13). But recently, it has been shown in Ref. 3 that it can be valid for the class of vehicle and mission in question here. In this reference, the necessary multitime-scale behavior of this vehicle's dynamics was demonstrated. And the energy-state solutions were judged to compare sufficiently favorably with a more accurate computational solution obtained via nonlinear programming to justify using the simpler approach in this sensitivity study.

The key result from the energy-state analysis is that the minimum-fuel trajectory results if the vehicle is operated at each energy level E such that $\mathrm{d}E/\mathrm{d}W_f$ is maximized. Thus, locally maximizing $\mathrm{d}E/\mathrm{d}W_f$ leads to the minimum-fuel trajectory for the SSTO mission. The optimal propulsion system (scramjet, rocket, etc.) can also be determined from this algorithm. That is, the propulsion system that yields the maximum $\mathrm{d}E/\mathrm{d}W_f$ at a given flight condition yields the optimum vehicle performance.

Finally, in this study, the scramjet-powered phase of the mission will be of primary interest. As discussed in Ref. 14, for flight between approximately Mach 6 and the edge of the (air-breathing) flight envelope, a scramjet engine can be the optimum propulsive mode, and the attention in this study will be focused on this phase of the trajectory. It will, therefore, be assumed that the vehicle is accelerated optimally up to Mach 6 by another propulsion system such as a turbo/ramjet.

SSTO Mission Characteristics for the Baseline Vehicle

The parameters defining the baseline configuration are listed in Table 1. Figure 7 presents the flight envelope for this vehicle over the range of Mach number being considered. Also shown are contours of constant energy gain per weight of fuel used, $\mathrm{d}E/\mathrm{d}W_f$, along with contours of constant energy height E. The constant E contours are shown as dash–dot lines, and note that these contours appear almost vertical in the hypersonic Mach regime.

Table 1 Baseline configuration data

W_{ave}	150,000 lb
A_e	$7.5 \times W_p$
A_n	5
W_a	20 ft
W_p	40 ft
W_{ab}	40 ft
l_1	75 ft
l_2	80.3 ft
l_3	150 ft
τ_1	15 deg
τ_2	14 deg

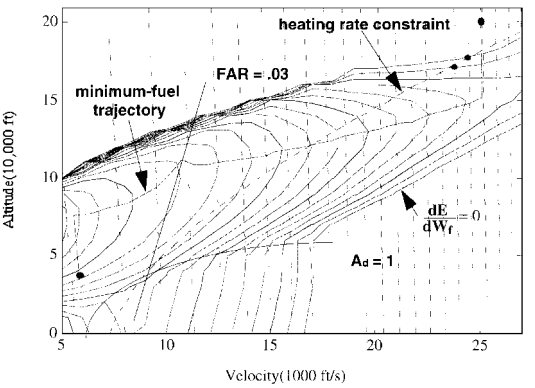

Fig. 7 Performance of baseline configuration.

The minimum-fuel trajectory is revealed in the same figure. For this trajectory, scramjet ignition is arbitrarily taken to occur at Mach 6 and 40,000-ft altitude (corresponding to an $E_0 = 5 \times 10^5$ ft). The initial phase of flight is a zoom climb at constant E to the optimum altitude of 75,000 ft, followed by a shallow, accelerating climb to slightly above Mach 25 at 150,000 ft (corresponding to an $E_f = 9.9 \times 10^6$ ft). Finally, a constant-energy zoom climb is performed to orbit insertion at 200,000 ft. The time required from scramjet ignition to orbit insertion is 1085 s, and the fuel required is 160,000 lb.

Also depicted in Fig. 7 are lines separating the regions of operation with regard to the engine diffuser limit and the FAR limit. One region of the envelope corresponds to flight with $A_d < 1$ (yielding $P_2 = 1$ atm), and one to flight with $A_d = A_{d\max} = 1$ ($P_2 > 1$ atm). Note the change in shape of the constant $\mathrm{d}E/\mathrm{d}W_f$ contours between these regions, and that the minimum-fuel trajectory takes place entirely in the variable-geometry region of the flight envelope. With regard to the other propulsion limit, the FAR in the combustor is either < 0.03 (for $M_3 = 1$) or the stoichiometric limit of 0.03 (for $M_3 > 1$). The point along the minimum-fuel trajectory at which FAR hits the stoichiometric limit is evident in the plot of the trajectory, as well as in the time histories shown in Fig. 8.

Finally, the contour in Fig. 7 labeled "heating rate constraint" reveals the effect of a limit on the maximum allowable heating rate experienced by the vehicle. The heat transfer rate near the stagnation region may be estimated from the following relation[15]:

$$\dot{Q} = 865\, R_n^{-\frac{1}{2}} (V/10^4)^{k_1} (\rho/\rho_0)^{k_2} \tag{12}$$

where R_n is a function of the vehicle's fineness ratio. For a given vehicle, Eq. (12) is of the form

$$\dot{Q} = C_4 \rho^{k_2} V^{k_1} \tag{13}$$

where C_4 is a geometry-dependent proportionality constant and k_1 and k_2 are taken to be 2.65 and 0.5, respectively. This relation was used to establish the constraint in Fig. 7, where the heating rate for the constraint shown corresponds to 5000 Btu/ft^2/s for the baseline configuration.

Now the optimal trajectory discussed violates this heating constraint. In fact, the maximum instantaneous heating rate experienced exceeds 10,000 Btu/ft^2/s. Further, the total heating load on the vehicle, the heat flux integrated over the entire trajectory, is 7.8×10^6 Btu/ft^2.

If, however, the maximum-heat flux is constrained to 5000 Btu/ft^2/s, the constrained minimum-fuel trajectory can also be identified from inspection of Fig. 7, using the energy-state algorithm. The first phase of this constrained trajectory is unchanged from the unconstrained case until the trajectory intersects the heating constraint. This intersection occurs at about 11,000 ft and 17,000 ft/s. Beyond this point, the constrained optimal trajectory lies on the constraint boundary. Note that this constrained trajectory cannot

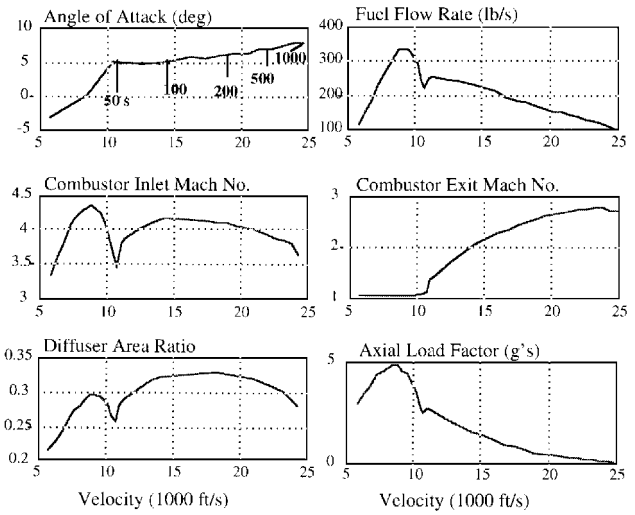

Fig. 8 Minimum-fuel trajectory histories, baseline configuration.

achieve orbital energy within the vehicle's flight envelope. Hence, conversion to rocket propulsion would be required to achieve orbital conditions in this case. The scramjet-powered phase of flight would terminate near the first dot on the heating constraint, and rocket power would be initiated at that point.

For this constrained trajectory, 182,000 lb of fuel are required for the scramjet phase of the trajectory, which is now 2035 s in duration. The effect of the heating constraint on mission performance is significant. Further, the total heating load experienced for the scramjet-powered phase has increased to 2.83×10^7 Btu/ft^2. This value is higher than that for the unconstrained case because the time of flight has been greatly increased. As discussed in Ref. 12, constraining heat load, rather than heating rate, leads to trajectories with much shorter time of flight but much greater heating rate. Thus, the minimum-fuel trajectory is a strong function of the type of heating constraint that is driving the structural design. For the remainder of this paper, we will consider only trajectories unconstrained by heating. These important effects will be further addressed in future work.

Figure 8 depicts the histories of key parameters along the original unconstrained trajectory. Shown are angle of attack, axial load factor, fuel-flow rate, combustor inlet and exit Mach number, and diffuser area ratio. Note that angle of attack is modest, the peak axial load factor is almost 5 g, and the average Mach number in the combustor is about 3.

As already noted, a variable diffuser is required to regulate combustor flow conditions. Of interest is the performance impact of such a diffuser, and a fixed-diffuser configuration was also evaluated. Here the diffuser ratio selected was 0.25, and the trajectory was recomputed holding the combustor inlet pressure constant at 1 atm from scramjet ignition at Mach 6 until achieving orbital energy. The time required for this scramjet-powered phase of flight increased to 1965 s, and 185,000 lb of fuel was used. Compared to the baseline configuration with variable diffuser, this represents an increase in time of flight of 820 s and 26,000 lb less weight to orbit.

Subsystem Efficiencies and Sizing

A partial list of fundamental phenomena that can affect subsystem efficiencies follows. Although the issues are categorized as either aerodynamic or propulsive, note that several could fall under both headings. Aerodynamics phenomena include boundary layer buildup and/or transition on forebody; three-dimensional aerodynamic effects; Z-turn force, inlet/cowl design; spillage of flow around engine inlet; control surface drag; and heating effects. Propulsion phenomena include cooling issues, in terms of fuel-flow rate required; engine temperature (structural) limits; total pressure (i.e., energy) losses in each stage of engine due to viscosity, shocks, heat transfer, etc.; combustion inefficiencies; exhaust plume effects, under- or overexpansion of air along afterbody; diffuser area ratio, nozzle area ratio; throttling, fuel scheduling; effect of different fuels; and engine inlet/cowl design, mass capture, and pressure recovery. In addition, there are sizing phenomena: vehicle geometry, lengths, and widths. The question is how to assess the effects of these phenomena on mission performance without having detailed models for the phenomena. The approach used here is to introduce some efficiency factors.

Each physical component of the vehicle is designed to accomplish a basic subtask that involves some fundamental physical process, such as mass capture, force generation, or energy conversion. A set of efficiencies will now be defined in terms of these basic subtasks.

Inlet Mass Capture

The basic process carried out by the engine inlet is capturing airflow with minimum energy loss. The mass-capture process depends on, for example, the boundary-layer buildup on the forebody and spillage at the inlet due to the bow shock detaching from the engine lip.[16,17] From conservation of mass, the ideal inlet mass flow rate $\dot{m}_{i,\text{ideal}}$ is

$$\dot{m}_{i,\text{ideal}} = \rho_i V_i A_i \tag{14}$$

and so let the actual mass capture be expressed as

$$\dot{m}_{i,\text{actual}} = \eta_m \dot{m}_{i,\text{ideal}} = \eta_m (\rho_i V_i A_i) \tag{15}$$

which defines the mass capture efficiency η_m.

Diffusion/Expansion

In each stage of the engine, diffuser, combustor, nozzle, energy losses will occur, for example, due to viscous effects, shocks, and heat transfer from the flow to the engine structure.[15–17] A loss in total energy leads to a loss in total pressure or total temperature. The basic process accomplished by both the diffuser and the nozzle is efficient pressure recovery. Therefore, for these two subsystems one may best define energy loss in terms of a loss in total pressure. Thus, for the total pressure across the diffuser, define

$$p_{t2} = \eta_d p_{t1} \tag{16}$$

where diffuser efficiency η_d is the diffuser total pressure ratio. Then we have

$$p_2\left\{1 + [(\gamma - 1)/2]M_2^2\right\}^{\gamma/(\gamma-1)} = \eta_d p_1\left\{1 + [(\gamma - 1)/2]M_1^2\right\}^{\gamma/(\gamma-1)} \tag{17}$$

Note that a variable-geometry diffuser is assumed here, which delivers a pressure of 1 atm into the combustor, or p_2. From the preceding equation, for a fixed value of p_2 (e.g., 1 atm) the Mach number into the combustor M_2 will be reduced as η_d is reduced.

The diffuser area ratio A_d that will deliver the desired p_2 is computed by enforcing mass conservation,[15] which results in the following:

$$\frac{\left\{1 + [(\gamma - 1)/2]M_2^2\right\}^{(\gamma+1)/(\gamma-1)}}{M_2^2} = A_d^2 \frac{\left\{1 + [(\gamma - 1)/2]M_1^2\right\}^{(\gamma+1)/(\gamma-1)}}{M_1^2}\left(\frac{p_{t2}}{p_{t1}}\right)^2$$

or, effectively,

$$\frac{\left\{1 + [(\gamma - 1)/2]M_2^2\right\}^{(\gamma+1)/(\gamma-1)}}{M_2^2} = (A_d \eta_d)^2 \frac{\left\{1 + [(\gamma - 1)/2]M_1^2\right\}^{(\gamma+1)/(\gamma-1)}}{M_1^2} \tag{18}$$

Inserting η_d from Eq. (17) into Eq. (18), it can be shown that to reduce M_2, ratio A_d must increase. Thus, the effect of diffuser p_t loss, for fixed p_2, is to reduce M_2 and increase A_d. From the Rayleigh flow combustion model, the reduction in M_2 equates to less energy obtained from combustion,[15] which, of course, leads to a reduction in thrust.

By similar arguments, the two governing equations across the nozzle are

$$\frac{\left\{1+[(\gamma-1)/2]M_4^2\right\}^{(\gamma+1)/(\gamma-1)}}{M_4^2} = (A_n\eta_n)^2\frac{\left\{1+[(\gamma-1)/2]M_3^2\right\}^{(\gamma+1)/(\gamma-1)}}{M_3^2} \tag{19}$$

and

$$p_4\left\{1+[(\gamma-1)/2]M_4^2\right\}^{\gamma/(\gamma-1)} = \eta_n p_3\left\{1+[(\gamma-1)/2]M_3^2\right\}^{\gamma/(\gamma-1)} \tag{20}$$

where nozzle efficiency η_n is defined as the nozzle total-pressure ratio p_{t4}/p_{t3}. For a fixed nozzle area ratio A_n, the effect of nozzle p_t loss is a reduction in both M_4 and p_4, which from Eq. (2) leads to less thrust.

Combustion

The combustor is designed to convert chemical energy in the fuel to heat energy of the working fluid. Fundamental causes of combustor energy loss include, for example, incomplete mixing of fuel and air, incomplete burning, and insufficient reaction and/or ignition times due to finite-rate chemistry.[7,18] The ideal total temperature rise of the working fluid due to combustion may be related to the FAR as follows:

$$\Delta T_{t,\text{ideal}} = \frac{\text{FAR}\,Q_r}{(1+\text{FAR})c_p} \tag{21}$$

This relation is based on the assumption that complete, ideal energy conversion occurs from the fuel to the working fluid.

Energy loss in the combustor may then be reflected in terms of loss in ΔT_t for a given FAR, or

$$\Delta T_{t,\text{actual}} = \eta_c \Delta T_{t,\text{ideal}} \tag{22}$$

Thus, the effect of combustor energy loss, as modeled herein, is to reduce the amount of energy release in the combustor, thus reducing thrust for a given fuel flow.

Afterbody/Nozzle Expansion

The afterbody/external nozzle subsystem affects the generation of the exhaust-plume force, for given flow conditions at the engine exit. Let the magnitude of F_{plume}, the vector sum of X- and Z-plume forces, be given by

$$|F_{\text{plume}}| = P_\infty l_2 W_{\text{ab}}\left[\frac{\bar{P}\,\ell n(\bar{P})}{(\bar{P}-1)}\right] \tag{23}$$

where $\bar{P} = P_e/P_\infty$. Let the reduction in $|\boldsymbol{F}_{\text{plume}}|$ due to any reason be reflected by a reduction in afterbody expansion efficiency η_e, defined by

$$|F_{\text{plume, actual}}| = \eta_e|F_{\text{plume, ideal}}| = (\eta_e W_{\text{ab}})P_\infty l_2\left[\frac{\bar{P}\,\ell n(\bar{P})}{(\bar{P}-1)}\right] \tag{24}$$

Aerodynamic Forces

The aerodynamic lifting surface(s) generate the required aerodynamic force F_{aero}, the vector sum of the lift and drag. And, for example, a phenomenon affecting F_{aero} is the pressure loss around the edges due to three-dimensional effects.[19] Any reduction in $|F_{\text{aero}}|$ then gives rise to an aerodynamic efficiency parameter η_a, where

$$|F_{\text{aero, actual}}| = \eta_a|F_{\text{aero, ideal}}| \tag{25}$$

Parasite Drag

Because of viscous effects, surface roughness, and control surface deflections, the parasite drag will increase above the ideal value. This would be associated with a concomitant increase in the profile drag coefficient C_{D_0}.

Table 2 Configuration matrix

Configuration	η_m	η_a	η_e	η_c	η_n	η_d	C_{D_0}	W_p	W_a	W_{ab}
Baseline	1	1	1	1	1	1	0.024	40	20	40
I	**0.9**	1	1	1	1	1	0.024	40	20	40
II	1	1	1	**0.9**	1	1	0.024	40	20	40
III	1	1	**0.9**	1	1	1	0.024	40	20	40
IV	1	**0.9**	1	1	1	1	0.024	40	20	40
V	1	1	1	1	1	1	**0.014**	40	20	40
VI	1	1	1	1	**0.9**	1	0.024	40	20	40
VII	1	1	1	1	1	**0.9**	0.024	40	20	40
VIII	1	1	1	1	1	1	0.024	**36**	20	40
IX	1	1	1	1	1	1	0.024	40	**18**	40
X	1	1	1	1	1	1	0.024	40	20	**36**

Sizing

Three sizing variables were utilized in the various expressions given for forces, fuel flow, etc. These were characteristic forebody width W_a, characteristic afterbody width W_{ab}, and characteristic propulsion system width W_p. Consequently, effects of changes in these characteristic lengths can also be evaluated, where these lengths have sizing implications. Note, however, that in the following treatment, no change in structural weight is considered when a characteristic length is varied.

Finally, in several expressions for forces, fuel flow, etc., the various efficiencies appeared in product terms involving one of these characteristic widths. For example, consider the following expression for the mass-capture efficiency:

$$\dot{m}_{i,\text{actual}} = \eta_m\,\dot{m}_{i,\text{ideal}} = \eta_m(\rho_i V_i A_i)_{\text{ideal}} \tag{26}$$

A change in this efficiency could also be interpreted as a reduction in effective inlet cross-sectional area. This area can be related to W_p through the expression

$$A_i = H_i W_p \tag{27}$$

where H_i is the engine inlet height. Consequently, several efficiency parameters already defined may be related to sizing variables or characteristics lengths (see Table 2). With this observation, the sizing implication of such efficiency changes is readily apparent.

Parametric Configuration Matrix and Mission Performance

The subsystem efficiencies and sizing parameters give rise to a matrix of vehicle configurations (Table 2) in which each configuration is defined in terms of a single perturbation from the baseline. This defines 10 perturbed configurations, denoted configurations I–X.

The minimum-fuel, scramjet-powered trajectories were determined for each of these configurations. In h–V coordinates, the optimal trajectories for configurations I–IV and VII–X are indistinguishable from that for the baseline configuration. (However, the time histories differ somewhat.) The optimal h-V trajectories for configurations V and VI were very similar to that of the baseline, but the altitude is about 1000 ft lower than that for the baseline at a given velocity. The flight envelopes (defined by the contour corresponding to $\mathrm{d}E/\mathrm{d}W_f = 0$) for configurations I–III, VI–VIII, and X are smaller than that of the baseline, whereas the envelopes for configurations IV, V, and IX are larger than baseline. Table 3 summarizes the key numerical results.

Subsystem Sensitivities

Under the sizing paradigm used in this analysis, an increase in the fuel weight required to reach orbit reduces payload to orbit pound for pound. Thus, the payload sensitivities for each perturbation may now be determined. For example, to first order the change in payload to orbit due to the aggregate effects of each perturbation could be expressed as follows:

$$\Delta_{\text{Payload}} = \sum_{i-1}^{6} S_i\Delta\eta_i + S_7\Delta C_{D_0} + \sum_{j=1}^{3} S_{j+7}\Delta W_j \tag{28}$$

Table 3 Subsystem performance implications

Configuration	Time, s	Fuel, lb	Effect
Baseline	1085 (total)	159,000 (total)	
I	+500	+47,000	Reduced mass capture
II	+560	+75,000	Imperfect combustion process
III	+120	+11,000	Reduced afterbody forces
IV	−215	−28,000	Reduced forebody aerodynamic forces
V	−490	−46,000	Decreased parasite drag
VI	+450	+71,400	Increased nozzle energy losses
VII	+225	+31,400	Increased diffuser energy losses
VIII	+500	+47,000	Propulsion-system width (size)
IX	−215	−28,000	Forebody width (size)
X	+120	+11,000	Afterbody width (size)
Fixed diff.	+880	+26,000	Fixed-geometry diffuser

Each sensitivity S_i is defined as the change in payload to orbit per percentage change in each of the 10 parameters, while holding the other parameters at their baseline values. From the results in Table 3, these subsystem sensitivities are

$$
\begin{aligned}
S_m &= 4700 \text{ lb per \% increase in } \eta_m \\
S_c &= 7500 \text{ lb per \% increase in } \eta_c \\
S_e &= 1100 \text{ lb per \% increase in } \eta_e \\
S_a &= -2800 \text{ lb per \% increase in } \eta_a \\
S_d &= 3140 \text{ lb per \% increase in } \eta_d \\
S_n &= 7140 \text{ lb per \% increase in } \eta_n \\
S_{CD_0} &= -110 \text{ lb per \% increase in } C_{D_0} \\
S_{Wp} &= 4700 \text{ lb per \% increase in } W_p \\
S_{Wa} &= -2800 \text{ lb per \% increase in } W_a \\
S_{Wab} &= 1100 \text{ lb per \% increase in } W_{ab}
\end{aligned}
$$

Based on these sensitivities, the greater importance of propulsive effects (i.e., mass capture, combustion and nozzle efficiencies) over aerodynamic effects (afterbody expansion, aerodynamic force production, and parasite drag) is apparent. Specifically, a 10% change in combustion efficiency leads to a 75,000-lb change in payload to orbit, which is 25% of the initial weight of the baseline configuration.

Of interest also is the fact that a reduction in aerodynamic force-generation capability, or a lower η_a, leads to increased mission performance. Further analysis reveals that the baseline vehicle is operating at a suboptimal L/D over a significant portion of the trajectory. Note that this does not imply the trajectory is suboptimal, but that the propulsive/aerodynamic tradeoff that leads to optimum mission-performance results involves operating at a suboptimal L/D. This result demonstrates that maximizing subsystem efficiency does not necessarily lead to maximum system efficiency.

As noted from Eqs. (8) and (9), in addition to L/D, T/W and SFC play a significant role and are angle-of-attack dependent. The required angle of attack at a particular flight condition is determined by enforcing force equilibrium. And if less lift is generated at a given angle of attack, due to a lower η_a, for example, then the vehicle must operate at a higher angle of attack. And the increase in performance with a lower η_a simply indicates that the propulsive-performance gains from operating the vehicle at higher angle of attack more than offset the loss from operating at a different L/D. This result suggests furthermore that there would be little performance penalty associated with a modest increase in the vehicle weight for the baseline configuration, because higher weight also leads to a higher trim angle of attack.

Finally, with regard to sizing, the results suggest that to enhance mission performance, effective forebody width W_a should be reduced, while effective propulsive width W_p and afterbody width W_{ab} should be increased. Such a configuration would have a lower slenderness ratio than the baseline, with strong emphasis on propulsive performance.

Conclusions

Air-breathing, SSTO vehicles have unique characteristics. Like aircraft, they rely on significant aerodynamic lift, and over a wide range of the flight envelope they have smaller thrust-to-weight ratios than rockets. But like rockets, their mission is to maximize payload into orbit, and so propulsive and structural efficiencies are extremely important. An energy-state analysis methodology was suggested for the performance analysis, and the sizing problem was formulated in terms of an optimization paradigm. For the class of vehicle considered, the minimum-fuel orbit-insertion trajectory is characterized more as an accelerating shallow climb in the atmosphere rather than either a cruise like an aircraft or a ballistic launch. Mission performance was evaluated, effect of heating constraints discussed, maximum orbital mass fractions determined, and configuration sensitivities assessed. Results based on the mission and vehicle model considered here indicate that the maximum achievable orbital mass fraction is a strong function of propulsion-system efficiencies and, to a lesser extent, the vehicle's aerodynamic efficiency. Furthermore, a mission-performance-optimized configuration would tend to have a low slenderness ratio, with maximum propulsive capability. Under the energy-state algorithm, the optimum propulsion system is that which delivers the maximum energy gain per weight of fuel used. Finally, heating constraints have a significant effect on operational efficiency and mission performance.

Acknowledgments

This research was supported by NASA Langley Research Center under Grant NAG 1-1540. The authors would like to thank the reviewers for their insightful comments.

References

[1] Anon., *Aviation Week and Space Technology*, Oct. 1990, p. 46.

[2] Schmidt, D. K., "Integrated Control of Hypersonic Vehicles," AIAA Paper 93-5091, Dec. 1993.

[3] Hermann, J. A., and Schmidt, D. K., "Fuel-Optimal Single-Stage-to-Orbit Mission Analysis of a Generic Hypersonic Vehicle," AIAA Paper 95-3372, Aug. 1995.

[4] Chavez, F. R., and Schmidt, D. K., "Analytical Aeropropulsive/Aeroelastic Hypersonic Vehicle Model with Dynamic Analysis," *Journal of Guidance, Control, and Dynamics*, Vol. 17, No. 6, 1994, pp. 1308–1319.

[5] Rogers, R. C., and Schexnayder, C. J., "Chemical Kinetic Analysis of Hydrogen-Air Ignition and Reaction Times," NASA TP 1856, July 1981.

[6] Schmidt, D. K., Mamich, H., and Chavez, F. R., "Dynamics and Control of Hypersonic Vehicles—The Integration Challenge for the 1990s," AIAA Paper 91-5057, Dec. 1991.

[7] Brewer, D. P., *Hydrogen Aircraft Technology*, CRC Press, Boca Raton, FL, 1991.

[8] Sachs, G., and Dinkelmann, M., "Trajectory Optimization for Reducing Coolant Fuel Losses of Aerospace Planes," AIAA Paper 95-3371, Aug. 1995.

[9] Corban, J. E., Calise, A. J., and Flandro, G. A., "Rapid Near-Optimal Aerospace Plane Trajectory Generation and Guidance," *Journal of Guidance, Control, and Dynamics*, Vol. 14, No. 6, 1991, p. 1181.

[10] Van Burin, M. A., and Mease, K. D., "Aerospace Plane Guidance Using Time-Scale Decomposition and Feedback Linearization," *Journal of Guidance, Control, and Dynamics*, Vol. 15, No. 5, 1992, p. 1166.

[11] Ardema, M. D., Bowles, J. V., Terjesen, E. J., and Whittaker, T., "Approximate Altitude Transitions for High-Speed Aircraft," *Journal of Guidance, Control, and Dynamics*, Vol. 18, No. 3, 1995, pp. 561–566.

[12] Lovell, T. A., Schmidt, D. K., and Chavez, F. R., "Using Trajectory Optimization to Determine Design Sensitivities for Single-Stage-to-Orbit Hypersonic Vehicles," AIAA Paper 93-4009, Aug. 1993.

[13] Bryson, A. E., Desai, M. N., and Hoffman, W. C., "Energy-State Approximation in Performance Optimization of Supersonic Aircraft," *Journal of Aircraft*, Vol. 6, No. 6, 1969, p. 481.

[14] Lovell, T. A., and Schmidt, D. K., "Effect of Aeropropulsive Interactions and Design Sensitivities on Optimal Hypersonic Ascent Trajectories," AIAA Paper 94-3524, Aug. 1994.

[15] Anderson, J. D., *Modern Compressible Flow with Historic Perspective*, 1st ed., McGraw–Hill, New York, 1982.

[16] Anon., *Hypersonic Technology for Military Application*, Committee on Hypersonic Technology, National Academy Press, Washington, DC, 1989.

[17] Bertin, J. J., Glowinski, R., and Periaux, J. (eds.), *Hypersonics: Defining the Hypersonic Environment*, Birkhauser, Boston, MA, 1989.

[18] Heiser, W. H., and Pratt, D. T., *Hypersonic Airbreathing Propulsion*, 1st ed., AIAA, Washington, DC, 1994.

[19] Anderson, J. D., *Fundamentals of Aerodynamics*, 2nd ed., McGraw–Hill, New York, 1991.

J. A. Martin
Associate Editor